Engineering the Electronic Structure of 2D WS$_2$ Nanosheets Using Co Incorporation as Co$_x$W$_{(1-x)}$S$_2$ for Conspicuously Enhanced Hydrogen Generation

Tofik Ahmed Shifa, Fengmei Wang, Kaili Liu, Kai Xu, Zhenxing Wang, Xueying Zhan, Chao Jiang, and Jun He*

Transition metal dichalcogenides (TMDs), as one of potential electrocatalysts for hydrogen evolution reaction (HER), have been extensively studied. Such TMD-based ternary materials are believed to engender optimization of hydrogen adsorption free energy to thermoneutral value. Theoretically, cobalt is predicted to actively promote the catalytic activity of WS$_2$. However, experimentally it requires systematic approach to form Co$_x$W$_{(1-x)}$S$_2$ without any concomitant side phases that are detrimental for the intended purpose. This study reports a rational method to synthesize pure ternary Co$_x$W$_{(1-x)}$S$_2$ nanosheets for efficiently catalyzing HER. Benefiting from the modification in the electronic structure, the resultant material requires overpotential of 121 mV versus reversible hydrogen electrode (RHE) to achieve current density of 10 mA cm^{-2} and shows Tafel slope of 67 mV dec^{-1}. Furthermore, negligible loss of activity is observed over continues electrolysis of up to 2 h demonstrating its fair stability. The finding provides noticeable experimental support for other computational reports and paves the way for further works in the area of HER catalysis based on ternary materials.

1. Introduction

Apart from being essential to several key industrial processes, hydrogen is proposed as the green energy carrier that would solve the global energy crisis and associated environmental problems.[1] Today, vast majority of hydrogen production is brought from steam reformation of hydrocarbons. But, this process is not only environmentally hazardous, but also suffers from the risk of scarcity due to nonrenewable resource consumptions.[2,3] The production of hydrogen should be in the most spotless way in order to insure the sustainability for its intended proposes.[4–6] Especially this era urges the scientific community to design a means to move away from fossil fuel dependence more than ever.[7] In response to this, it has been found that hydrogen gas can be eco-friendly produced by electrocatalytic splitting of water into its constituent elements—hydrogen and oxygen.[5,8] Pt-based electro-catalysts exhibit high performance to put in action the hydrogen evolution reaction (HER) in acidic solution.[9–11] However, this does not go in accordance with the fact on the ground to tangibly solve the existing problem in scalable manner. Exploration of earth abundant and inexpensive materials is, therefore, the way forward. Presently, owing to their intriguing physical and chemical properties[11–15] and also inspired by nature,[16] edge

T. A. Shifa, F. M. Wang, K. Liu, K. Xu, Dr. Z. Wang,
X. Zhan, Prof. C. Jiang, Prof. J. He
CAS Center for Excellence in Nanoscience
National Center for Nanoscience and Technology
Beijing 100190, China
E-mail: hej@nanoctr.cn

T. A. Shifa, F. M. Wang, K. Liu, K. Xu, Dr. Z. Wang,
X. Zhan, Prof. J. He
CAS Key Laboratory of Nanosystem and Hierarchical Fabrication
National Center for Nanoscience and Technology
Beijing 100190, China

T. A. Shifa, F. M. Wang, K. Liu, K. Xu
University of Chinese Academy of Sciences
Beijing 100049, China

exposed transition metal dichalcogenides (TMDs) are thought to be active for catalyzing HER process. Various strategies have been followed to develop TMD-based electrocatalysts including defect engineering,[17–20] edge engineering,[21–26] and phase engineering[27–31] based on MoS_2, WS_2, etc. Of the many approaches to improve the intrinsic activity of TMD's catalysis, doping of another atom is believed to play a significant role in optimizing the free energy of hydrogen adsorption.[10,32,33] As such, experimental and theoretical studies reveal that metal[34–47] or chalcogen[48–53] doped TMDs are more active than undoped binary ones. Particularly, Co exhibits most significant promotional effect in catalyzing HER as evidenced in FeS_2,[34] MoS_2,[47,48,54] WS_x,[44] and MoS_x[45] by lowering the free energy barrier for H adsorption.[32] Bonde et al.[47] put forward that cobalt atom in WS_2 leads to the decrement of the free energy of hydrogen adsorption on the exposed S-edge thereby creation of new sites with higher activity than pristine WS_2 via density functional theory (DFT) simulation and calculation. A cathode built from such material will, therefore, benefit the advantage of electronic perturbation induced by metal doping which would ultimately boost the HER activity. Guided by this, sulfidation of co-impregnated aqueous solution of cobalt and tungsten precursors is employed by different groups[46,55,56] with an aim of synthesizing co-doped WS_2. However, cobalt is sulfided first and results in the formation of catalytically inactive Co_9S_8 as a side product. In this case, the difficulty in simultaneous sulfidation behavior of W and Co, which tends to from CoS_x instead of Co–W–S,[47,55] hinders the improvement of Co-doped WS_2 nanomaterials for HER. It has, therefore, remained challenging to synthesize pure $Co_xW_{(1-x)}S_2$. Thus, in order to realize the effect of Co in WS_2 for HER catalysis, a systematic route that would not result in the formation of any side phase is highly essential. Herein, we devise a rational method to circumvent this problem by transferring Co from CoO/carbon fiber (CF) nanowire to already formed WS_2/W foil nanosheets. This route, due to the absence of simultaneous sulfurization, paves easy way for cobalt atom to get into WS_2 and forms ternary $Co_xW_{(1-x)}S_2$ nanosheet. Moreover, it does not only eliminate the formation of side products, but also keeps the nanosheets morphology of WS_2 in the final product that greatly helps to maximize the geometrical exposure of active edges. In fact, dopants avail themselves at a very close position to the surface of the material in the case of nanosheets morphology.[33] What's more, the substrate is also the source of W in the ultimate formation of $Co_xW_{(1-x)}S_2$ nanosheet which guarantees the uniform fastening of the electrocatalysts on the substrate and forms suitable scaffold for the built ternary material. As such, the content of Co reveals significant promotional effect as evidenced from the observed HER performance of $Co_xW_{(1-x)}S_2$ with a potential of 121 mV versus RHE at 10 mA cm^{-2} and small Tafel slope of 67 mV dec^{-1}. To the best of our knowledge, this is the first report demonstrating the noticeable effect of cobalt in systematically designed ternary $Co_xW_{(1-x)}S_2$ nanosheet which represents the state-of-the-art in so far WS_2-based electrocatalysts are concerned.

## 2. Results and Discussion

Vertically aligned triangular WS_2 nanosheets[57] on W foil and densely populated CoO nanowire arrays[58] on carbon fiber were grown in our previous works. In order to realize the homogeneous doping of Co atoms into the WS_2 nanosheets, systematic Co transfer was made through further sulfurization via two zone chemical vapor deposition (CVD) method in which S powder was loaded in the front zone whereas the as-grown CoO/CF nanowire and WS_2/W foil nanosheets were kept nearby one another at the back zone of Ar saturated reactor tube (**Figure 1**). The heating temperature is crucial during this reaction process. Temperature of 800 °C was set at the back zone to put in action the formation of ternary $Co_xW_{(1-x)}S_2$ and we found that lower temperatures are not energetic enough to liberate Co from the carbon fiber to WS_2
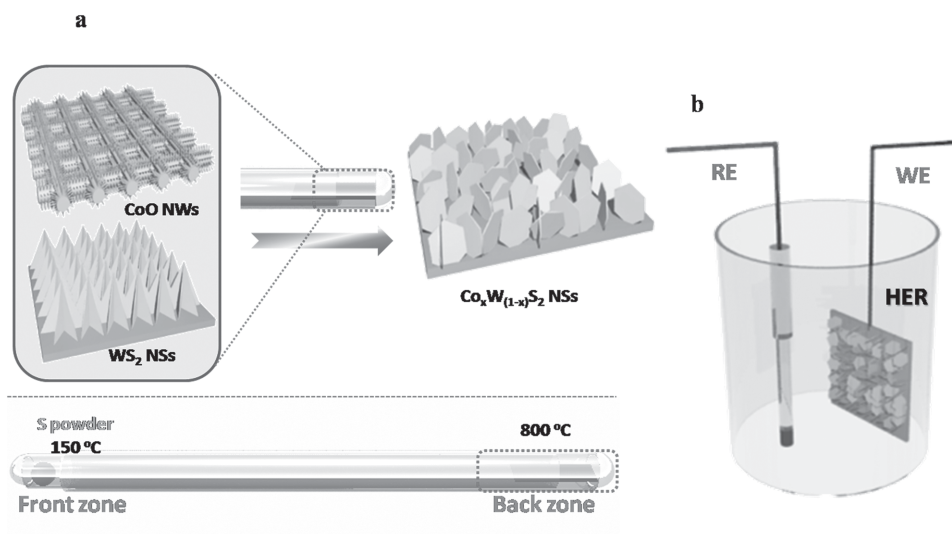

Figure 1. a) Schematic illustrating the transfer of cobalt atom from CoO NW grown on carbon fiber to WS_2 nanosheet grown on W foil in a typical two zone CVD furnace. b) The HER setup when the as-obtained ternary $Co_xW_{(1-x)}S_2$ is used as electrocatalysts. WE = working electrode, RE = Reference electrode.

on the W foil (Figure S2, Supporting Information). On the one hand, the CoO nanowires completely destroyed leaving almost bare carbon fiber (Figure S3, Supporting Information) after such transfer operation. On the other hand, the WS_2/W foil nanosheets were found to be doped with small content of cobalt. Had Co–W bimetallic oxide been sulfurized altogether, it would have been impossible to get pure Co-doped WS_2 due to the significantly different sulfurization temperatures of tungsten and cobalt oxides. The morphology and crystal structure of the as-synthesized nanosheets were studied by using scanning electron microscope (SEM) and high resolution transmission electron microscope (HRTEM), both of which are equipped with energy dispersive X-ray spectroscopy (EDX). It is apparent from **Figure 2** that the nanosheets were grown uniformly on the entire surface of the W foil. The composition of the as-grown material is revealed as Co, W, and S with atomic ratio close to 1:32:66 corresponding to a value of 0.03 for "x" in $Co_xW_{(1-x)}S_2$. TEM–EDX elemental mappings of Co, W, and S were taken from the marked region of the nanosheets. Conspicuously, uniform distribution of the constituents can be realized in the as synthesized $Co_xW_{(1-x)}S_2$ nanosheet. The HRTEM and corresponding selected area electron diffraction pattern reveal a high quality hexagonal crystal structure in which the obtained lattice space of 0.27 nm can be assigned to the (100) plane in hexagonal WS_2. This plane also appears at 2θ value of 32.93° in the X-ray diffraction (XRD) pattern. Further crystallographic information was obtained from XRD patterns which are presented in Figure S1 in the Supporting Information. The diffractograms can be mainly indexed to hexagonal WS_2 (PDF # 87-2417).

There is no obvious peak showing the formation of Co_9S_8 or any phase corresponding to CoS_x suggestive of our successful doping strategy. The characterization with Raman spectroscopy measurement was also performed to see the effect of Co doping in the characteristics Raman shifts that are pertinent to WS_2. Accordingly, **Figure 3**a clearly depicts the Raman shifts at 350 and 419 cm^{-1} which are due to A_{1g} and E_{2g} modes of vibrations respectively. It is interesting to note that, there exists a shift of ≈ 2 cm^{-1} in the observed Raman peaks of $Co_xW_{(1-x)}S_2$ as compared to pure WS_2 nanosheets. These kinds of peak shifts are quite common for small content of dopant atoms in the host material as reported elsewhere.[59–61] Here, the result from XRD diffractogram can be corroborated from the fact that Co doping did not change the crystal structure of WS_2 aside from inducing modifications in the electronic structure. The elemental states of $Co_xW_{(1-x)}S_2$ nanosheet were identified by employing X-ray photoelectron spectroscopy (XPS). As depicted in Figure 3b–d, the clear signals for W 4f, S 2p, and Co 2p are evidenced. The peaks observed at binding energies of 32.29 and 34.39 are attributable to W $4f_{7/2}$ and W $4f_{5/2}$ states and those at 161.9 and 163 are implying S $2p_{3/2}$ and S $2p_{1/2}$ states. The characteristics of W^{4+} species are apparent from the XPS observation as it agrees well to the reported values of binding energies for W in $CoWS_x$ type materials.[44] XPS profile of Co 2p shows a peak at binding energy of 778.7 which is suggestive for the presence of Co in $Co_xW_{(1-x)}S_2$. This value is very close to the one reported for Co 2p in CoWSx, CoMoP, or CoMoS phases.[44,62–64] Here also, the absence of any cobalt sulfide phase, like Co_9S_8, can be substantiated as there is no peak corresponding to Co

Element	Atomic%
S	66.77
Co	1.34
W	31.88
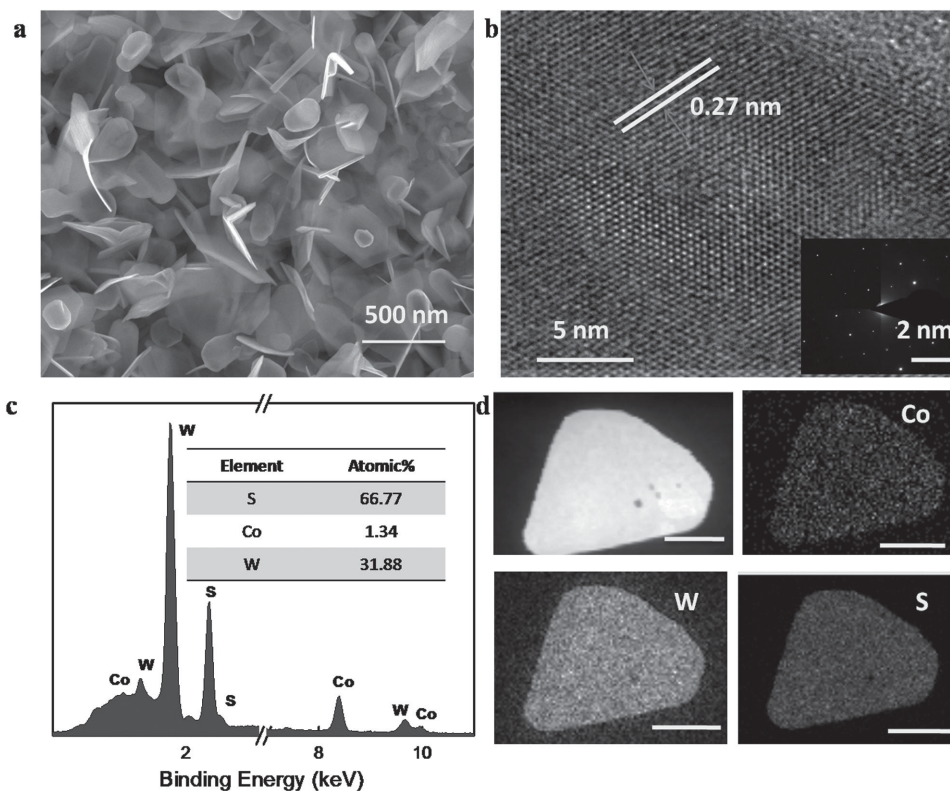
Figure 2. a) SEM and b) HRTEM (inset showing the SEAD pattern) image of the ternary $Co_xW_{(1-x)}S_2$. c) EDX spectrum of the ternary $Co_xW_{(1-x)}S_2$. d) TEM–EDX elemental mapping (Scale bar = 100 nm) of Co, W, and S in $Co_xW_{(1-x)}S_2$ nanosheet.
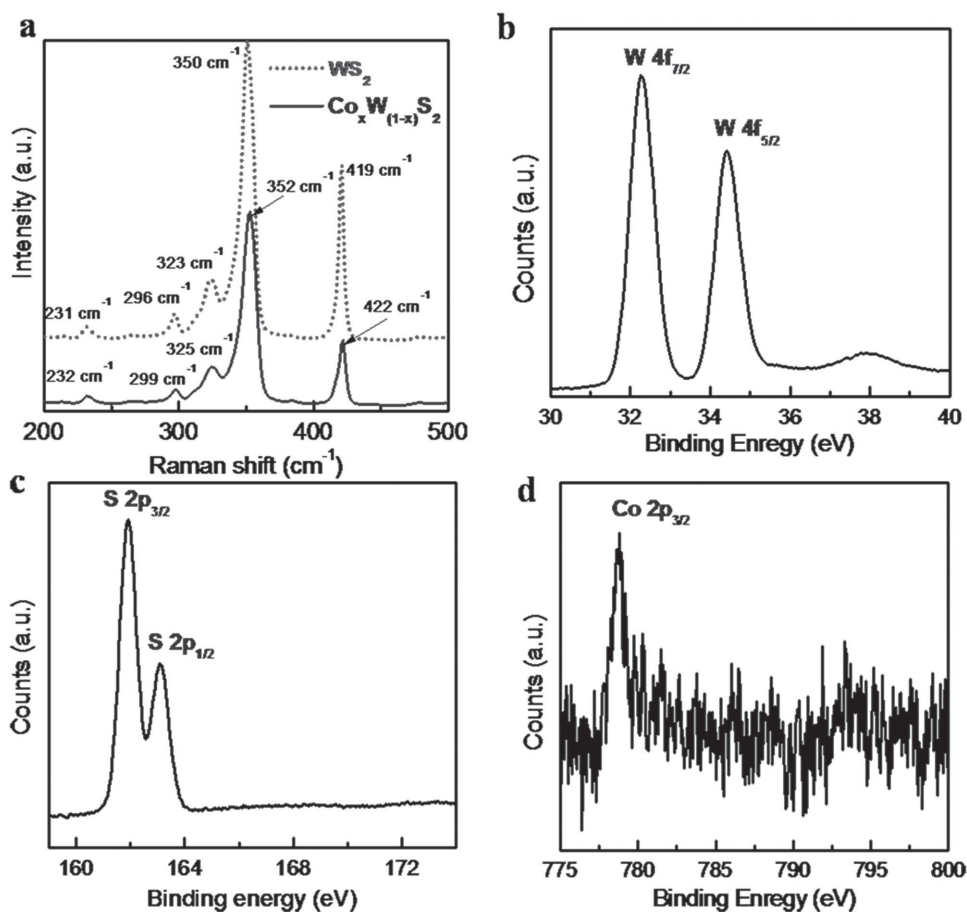
Figure 3. a) Raman spectrum of WS_2 and $Co_xW_{(1-x)}S_2$ nanosheets. High resolution XPS spectra of b) W 4f region, c) S 2p region, and d) Co 2p region of $Co_xW_{(1-x)}S_2$ nanosheets.

(at 778.1 ± 0.1 eV) for our case. XPS depth profiling of Co in WS_2 was investigated at different etching times (up to 900 s) to acquire information about the dopant's interior distribution. Successive etching brings complete removal of surface contamination that would ultimately expose the subsurface of Co 2p region.[65,66] Figure S4 in the Supporting Information illustrates similar binding energies for various spectra obtained at different etching times (and hence different depth). It appears conclusive that the uniform distribution of cobalt extends to the interior of WS_2 matrix. Thus, our findings from XPS further confirm the successful doping of Co into WS_2 nanosheet.

Having characterized and confirmed the successful doping of Co into hexagonal WS_2 nanosheet, we measured the electrocatalytic performance to see how Co improved the catalytic activity of WS_2 for hydrogen evolution reaction. Linear sweep voltammetry (LSV) was performed at scan rate of 5 mV s^{-1} in N_2 saturated 0.5 M H_2SO_4 using saturated calomel electrode (SCE) as reference electrode, graphite rod as counter electrode and the material under investigation as working electrode. The Potentials were referenced to a reversible hydrogen electrode (RHE) and the displayed polarization curves are iR corrected. The HER performance of Pt foil as bench mark catalyst was evaluated under similar condition. As expected, **Figure 4**a shows excellent performance for Pt foil. The promotional effect of Co is obvious from the polarization

curve demonstrating significantly enhanced performance as compared to pure WS_2. As such, $Co_xW_{(1-x)}S_2$ requires overpotential of 121 mV to reach a current density of 10 mAcm^{-2}, much lower than that of WS_2 (236 mV). For a better representation of practical water electrocatalysis, we run chronopotentiometric measurement at constant current density of 10 mA cm^{-2} for 2 h of continuous reaction. Except for some minor decay, stable catalytic activity at the selected bench mark current density is evident from Figure S6 in the Supporting Information. This enhancement clearly conveys the efficient role of Co in increasing the catalytic activity of WS_2 nanosheet. Tafel slope, providing information about kinetics of charge transfer process, was extracted from the polarization curve by fitting the linear part of the Tafel plots as per the Tafel equation (Figure 4b). Figure 4b shows the fact that the Tafel slope of $Co_xW_{(1-x)}S_2$ is calculated to be 67 mV dec^{-1}, further reflecting the promotional effect of Co as smaller Tafel slope indicates a faster increment of HER velocity with increasing potential.[67] Additionally, the measurement with respect to electrochemical impedance spectroscopy (EIS) at 0.1 V versus RHE was performed to further solidify the reason behind performance enhancement after Co-doping from the basis of the improved conductivity. To this aim, Nyquist plot was obtained as depicted in Figure 4c and the corresponding equivalent circuit model (Inset of Figure 4c) reveals a circuit consisting of a series resistance (Rs), constant phase element and charge
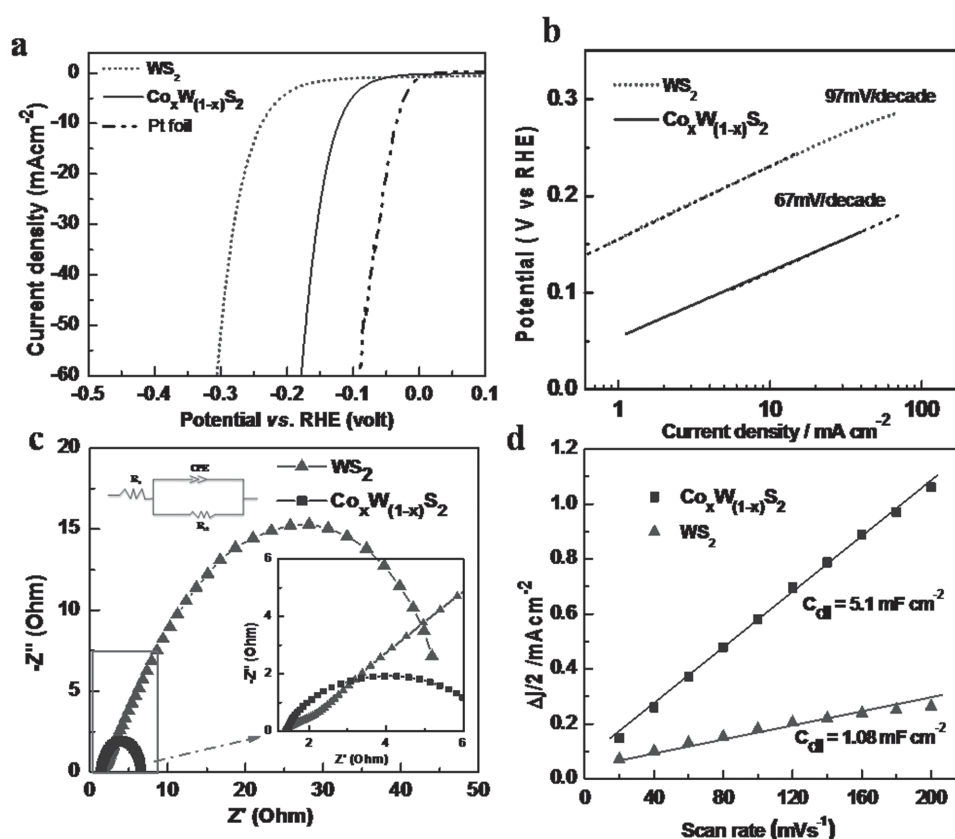
Figure 4. Electrochemical measurements of samples for catalyzing HER: a) polarization curves. b) Tafel slopes. c) Electrochemical impedance spectroscopy, Nyquist plots, and d) Cdl estimation reflecting the electrochemical active surface area.

transfer resistance (Rct). Notably, the smaller values of R_s and R_{ct} for $Co_xW_{(1-x)}S_2$ (0.83 and 5.38 Ω respectively) as compared to that of WS_2 (1.29 and 50.3 Ω, respectively) show how efficiently Co promote the electron charge transfer of HER on the surface of $Co_xW_{(1-x)}S_2$ nanosheets. To compare the electrochemical active surface areas (ECSA) of $Co_xW_{(1-x)}S_2$ and WS_2 electrodes, the determination of double layer capacitance (C_{dl}) was made by running cyclic voltammetry at various scan rates (20–200 mV s^{-1}) in the potential range of 0.1–0.2 V versus RHE (Figure S3, Supporting Information). The halves of the differences of anodic and cathodic current densities were plotted against the scan rates to give the graph as shown

in Figure 4d. The slope of such plot corresponds to the value of C_{dl} which in turn reflects the effective surface area. It is evident in the Figure that the ECSA of $Co_xW_{(1-x)}S_2$ is 5.1 m F cm^{-2} which is approximately five times that of pristine WS_2. This result conspicuously evidences that Co doping increased the number of active sites. As reported,[47] the creation of new sites on S edges with higher activity is among the phenomenon expected after incorporation of Co into WS_2 matrix.

Stability is another important aspect to be given due consideration while evaluating electrocatalytic performance of a given catalyst. **Figure 5**a shows the generation of H$_2$ without any decay up to 2 h of continuous reaction. The alternate
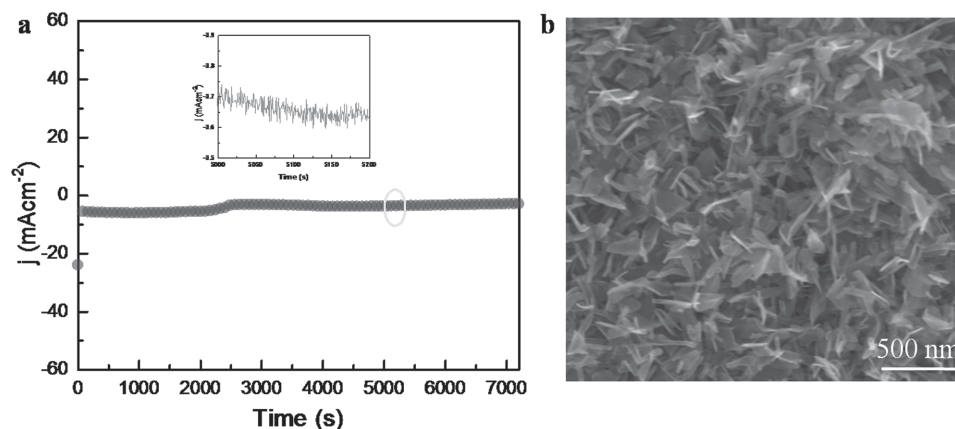

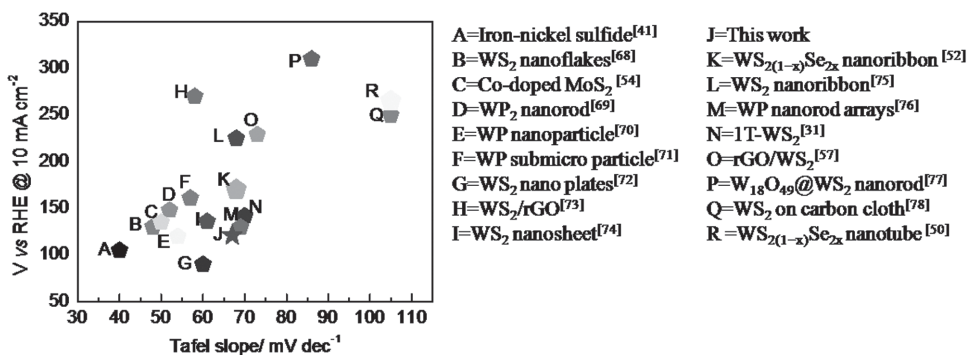**Figure 5.** a) Durability test of the electrocatalyst obtained from amperometric *I–t* run at −0.15V versus RHE in N$_2$ saturated 0.5 M H$_2$SO$_4$.b) SEM image of the ternary $Co_xW_{(1-x)}S_2$ nanosheets after stability test.

Figure 6. Comparison of the fabricated $Co_xW_{(1-x)}S_2$ nanosheet with the state-of-the-art HER electrocatalysts in terms of Tafel slope and the overpotential required to achieve current density of 10 mA cm^{-2}. Data from references [31–78]

process of bubble accumulation and release can be realized from the serrate shape of chrono-amperometric I–t curve (Inset of Figure 5a). The retentive nature of the ternary electro catalyst is also manifested from the preserved morphology in Figure 5b. Moreover, we also performed accelerated CV scanning for 1000 cycles at scan rate of 100 mV s^{-1} and found that only a minor deterioration in the cathodic current (Figure 5S). In general, the observed performance is fairly comparable with other recently produced tungsten-based materials interms of the Tafel slope and the potential required to achieve benchmark current density of 10 mA cm^{-2} (**Figure 6** and Table S1, supporting infromation).

3. Conclusion

In summary, We, for the first time, incorporated Co into WS$_2$ nanosheet without any concomitant side phases and show the efficient role of ternary $Co_xW_{(1-x)}S_2$ in catalyzing HER. The new active sites emanated as a result of Co incorporation are believed to play significant role for the observed overall HER performance of $Co_xW_{(1-x)}S_2$ which by far outperformed the pristine WS$_2$. This work provides further experimental support for theoretical speculations reported previously and paves the way for future works based on ternary materials.

4. Experimental Section

Synthesis of WS$_2$ Nanosheet on W foil: WS$_2$ nanosheet with mass density of 0.08 g cm^{-2} was obtained from the sulfurization of self-seeded WO$_3$ nanotree grown hydrothermally (Supporting information). In the typical synthesis, a two zone CVD was used, wherein the front zone is loaded by S powder and the as-prepared WO$_3$ nanotree was placed at the back zone. The tube was flushed with Ar gas three times and pumped into a vacuum lower than 1 Pa in order to create oxygen free environment. The temperature of back zone was raised to 800 °C at a heating rate of 20 °C min^{-1} while the front zone began to increase in temperature above the melting point of S (150 °C) at a rate of 10 °C min^{-1}. The conversion process was maintained for 60 min with 50 sccm Ar gas flow. Finally, the furnace was allowed to cool to room temperature.

Synthesis of CoO Nanowire on CF: A piece of CF was first orderly washed by acetone, ethanol, and ultrapure water in a sonicator

followed by drying at 60 °C. The cleaned CF was seeded with the precursors to grow CoO NWr by soaking in ethanolic solution of 1.90 g CoCl$_2$ and 2.424 g CO(NH$_2$)$_2$ for 10 min, then calcined under a flow of Ar gas at 450 °C for 4 h to form a seed layer. The seeded CF was then immersed into a 50 mL Teflon-lined stainless steel autoclave containing aqueous solution of 1.90 g CoCl$_2$ and 2.424 g CO(NH$_2$)$_2$ and the whole content was heated in an oven at 90 °C for 4 h. Finally, the CF was taken out and annealed at 500 °C for 4 h under the flow of Ar to obtain CoO NW/CF with mass density of 1.7 mg cm^{-2}.

Synthesis of $Co_xW_{(1-x)}S_2$ Nanosheet : A CVD method was employed to systematically transfer cobalt from the as-grown CoO NWr to WS$_2$ nanosheet. Typically, S powder was loaded on the front zone whereas the as-obtained CoO NWr and WS$_2$ nanosheet were placed at the back zone in an Ar saturated CVD tube. The two zones are 25 cm apart. The starting materials placed at either zone were kept at the thermal center of fixed distance from one another. And the distance between CoO NWr and WS$_2$ nanosheet in the back zone was kept close enough for ease of Co transfer. With such arrangement, the temperature of the front zone was raised to 150 °C at a rate of 10 °C min^{-1} and that of the back zone was raised to 800 °C at heating rate of 20 °C. The transfer process was maintained for 30 min with 50 sccm Ar gas flow. Finally, the furnace was allowed to cool to room temperature.

Characterizations: The morphologies were visualized by using Hitachi S4800 SEM and FEI Tecnai F20 TEM operated at 200 kV. STEM–EDX elemental mapping was performed on JEM-2100F (200 kV). Confocal microscope-based Raman spectrometer (Renishaw InVia) was employed in ambient air environment with an excitation laser line of 532 nm to acquire the Raman spectra of the as-synthesized samples. X-ray diffraction patterns were gathered from XRD (D/MAX-TTRIII (CBO) diffractometer) using Cu Kα radiation (λ = 1.5418 Å). XPS spectra were recorded on ESCALAB 250 Xi system of Thermo Scientific, where the analysis chamber was 1.5 × 10^{-9} Mbar and the X-ray spot was 500 μm.

Electrochemical Measurements: A typical three-electrode set-up was utilized for electrochemical measurement with CHI 660D potentiostat (CH Instruments, China). All measurements of the HER activity were conducted using a 0.5 M H$_2$SO$_4$ electrolyte under continuous purging with 99.999% of N$_2$ gas. The as-synthesized ternary $Co_xW_{(1-x)}S_2$, SCE and graphite rod served as working electrode, reference electrode, and counter electrode respectively. The electrocatalytic activities of these samples were examined by polarization curves using LSV at a scan rate of 5 mV s^{-1}.

The polarization curves demonstrated were corrected for iR losses. All potentials were calibrated to a RHE. The data for EIS was gathered in the frequency range from 0.01 Hz to 0.5 MHz with voltage of 0.1 V versus RHE. The estimation of electrochemical active surface area was done by running cyclic voltammeter at 10 various scan rates (20–200 mV s^{-1}) in the potential range of 0.1–0.2 V versus RHE.

Supporting Information

Supporting Information is available from the Wiley Online Library or from the author.

Acknowledgements

[1] G. W. Crabtree, M. S. Dresselhaus, M. V. Buchanan, *Phys. Today* **2004**, *57*, 39.
[2] B. E. Logan, *Environ. Sci. Technol.* **2004**, *38*, 160A.
[3] J. R. Rostrup-Nielsen, *Catal. Rev.* **2004**, *46*, 247.
[4] J. A. Turner, *Science* **2004**, *305*, 972.
[5] M. G. Walter, E. L. Warren, J. R. McKone, S. W. Boettcher, Q. Mi, E. A. Santori, N. S. Lewis, *Chem. Rev.* **2010**, *110*, 6446.
[6] D. Larcher, J. M. Tarascon, *Nat. Chem.* **2015**, *7*, 19.
[7] P. Rogers, *Environ. Sci. Technol.* **1991**, *25*, 580.
[8] H. B. Gray, *Nat. Chem.* **2009**, *1*, 7.
[9] J. Greeley, T. F. Jaramillo, J. Bonde, I. B. Chorkendorff, J. K. Norskov, *Nat. Mater.* **2006**, *5*, 909.
[10] J. D. Benck, T. R. Hellstern, J. Kibsgaard, P. Chakthranont, T. F. Jaramillo, *ACS Catal.* **2014**, *4*, 3957.
[11] F. Wang, T. A. Shifa, X. Zhan, Y. Huang; K. Liu; Z. Cheng, C. Jiang, J. He, *Nanoscale* **2015**, *7*, 19764.
[12] M. Chhowalla, H. S. Shin, G. Eda, L.-J. Li, K. P. Loh, H. Zhang, *Nat. Chem.* **2013**, *5*, 263.
[13] M. Xu, T. Liang, M. Shi, H. Chen, *Chem. Rev.* **2013**, *113*, 3766.
[14] A. K. Geim, I. V. Grigorieva, *Nature* **2013**, *499*, 419.
[15] T. F. Jaramillo, K. P. Jørgensen, J. Bonde, J. H. Nielsen, S. Horch, I. Chorkendorff, *Science* **2007**, *317*, 100.
[16] B. Hinnemann, P. G. Moses, J. Bonde, K. P. Jørgensen, J. H. Nielsen, S. Horch, I. Chorkendorff, J. K. Nørskov, *J. Am. Chem. Soc.* **2005**, *127*, 5308.
[17] J. Xie, H. Zhang, S. Li, R. Wang, X. Sun, M. Zhou, J. Zhou, X. W. Lou, Y. Xie, *Adv. Mater.* **2013**, *25*, 5807.
[18] J. Xie, J. Zhang, S. Li, F. Grote, X. Zhang, H. Zhang, R. Wang, Y. Lei, B. Pan, Y. Xie, *J. Am. Chem. Soc.* **2013**, *135*, 17881.
[19] J. Hong, Z. Hu, M. Probert, K. Li, D. Lv, X. Yang, L. Gu, N. Mao, Q. Feng, L. Xie, J. Zhang, D. Wu, Z. Zhang, C. Jin, W. Ji, X. Zhang, J. Yuan, Z. Zhang, *Nat. Commun.* **2015**, *6*, 6293.
[20] W. Zhou, X. Zou, S. Najmaei, Z. Liu, Y. Shi, J. Kong, J. Lou, P. M. Ajayan, B. I. Yakobson, J.-C. Idrobo, *Nano Lett.* **2013**, *13*, 2615.
[21] D. Y. Chung, S.-K. Park, Y.-H. Chung, S.-H. Yu, D.-H. Lim, N. Jung, H. C. Ham, H.-Y. Park, Y. Piao, S. J. Yoo, Y.-E. Sung, *Nanoscale* **2014**, *6*, 2131.
[22] Z. Wu, B. Fang, Z. Wang, C. Wang, Z. Liu, F. Liu, W. Wang, A. Alfantazi, D. Wang, D. P. Wilkinson, *ACS Catal.* **2013**, *3*, 2101.
[23] H. Wang, Q. Zhang, H. Yao, Z. Liang, H.-W. Lee, P.-C. Hsu, G. Zheng, Y. Cui, *Nano Lett.* **2014**, *14*, 7138.
[24] T. P. Nguyen, S. Choi, J.-M. Jeon, K. C. Kwon, H. W. Jang, S. Y. Kim, *J . Phys. Chem. C* **2016**, *120*, 3929.
[25] Y. Yang, H. Fei, G. Ruan, C. Xiang, J. M. Tour, *Adv. Mater.* **2014**, *26*, 8163.
[26] Y. Yang, H. Fei, G. Ruan, Y. Li, J. M. Tour, *Adv. Funct. Mater.* **2015**, *25*, 6199.
[27] X. Guo, G. Yang, J. Zhang, X. Xu, *AIP Adv.* **2015**, *5*, 097174.
[28] D. Voiry, H. Yamaguchi, J. Li, R. Silva, D. C. B. Alves, T. Fujita, M. Chen, T. Asefa, V. B. Shenoy, G. Eda, M. Chhowalla, *Nat. Mater.* **2013**, *12*, 850.
[29] D. Voiry, M. Salehi, R. Silva, T. Fujita, M. Chen, T. Asefa, V. B. Shenoy, G. Eda, M. Chhowalla, *Nano Lett.* **2013**, *13*, 6222.
[30] M. A. Lukowski, A. S. Daniel, F. Meng, A. Forticaux, L. Li, S. Jin, *J. Am. Chem. Soc.* **2013**, *135*, 10274.
[31] M. A. Lukowski, A. S. Daniel, C. R. English, F. Meng, A. Forticaux, R. J. Hamers, S. Jin, *Energy Environ. Sci.* **2014**, *7*, 2608.
[32] Y. Zheng, Y. Jiao, M. Jaroniec, S. Z. Qiao, *Angew. Chem. Int. Ed.* **2015**, *54*, 52.
[33] D. Voiry, J. Yang, M. Chhowalla, *Adv Mater.* **2016**. DOI: 10.1002/adma.201505597.
[34] D. Y. Wang, M. Gong, H. L. Chou, C. J. Pan, H. A. Chen, Y. Wu, M. C. Lin, M. Guan, J. Yang, C. W. Chen, Y. L. Wang, B. J. Hwang, C. C. Chen, H. Dai, *J. Am. Chem. Soc.* **2015**, *137*, 1587.
[35] Z. Peng, D. Jia, A. M. Al-Enizi, A. A. Elzatahry, G. Zheng, *Adv. Energy Mater.* **2015**, *5*, 1402031.
[36] L. Wang, Z. Sofer, J. Luxa, M. Pumera, *Adv. Mater. Int.* **2015**, *2*, 1500041.
[37] D. Kong, J. J. Cha, H. Wang, H. R. Lee, Y. Cui, *Energy Environ. Sci.* **2013**, *6*, 3553.
[38] G. Berhault, L. C. Araiza, A. D. Moller, A. Mehta, R. R. Chianelli, *Catal. Lett.* **2002**, *78*, 81.
[39] M. Brorson, A. Carlsson, H. Topsøe, *Catal. Today* **2007**, *123*, 31.
[40] G. Berhault, M. P. De la Rosa, A. Mehta, M. J. Yácaman, R. R. Chianelli, *Appl.Catal. A: General* **2008**, *345*, 80.
[41] Long, G. Li, Z. Wang, H. Zhu, T. Zhang, S. Xiao, W. Guo, S. Yang, *J. Am. Chem. Soc.* **2015**, *137*, 11900.
[42] H. Wang, C. Tsai, D. Kong, K. Chan, F. Abild-Pedersen, J. K. Nørskov, Y. Cui, *Nano Res.* **2015**, *8*, 566.
[43] D. Wang, X. Zhang, Y. Shen, Z. Wu, *RSC Adv.* **2016**, *6*, 16656.
[44] P. D. Tran, S. Y. Chiam, P. P. Boix, Y. Ren, S. S. Pramana, J. Fize, V. Artero, J. Barber, *Energy Environ. Sci.* **2013**, *6*, 2452.
[45] D. Lim, H. Hwang, T. Kim, S. E. Shim, S.-H. Baeck, *J. Nanosci. Nanotechnol.* **2015**, *15*, 8257.
[46] D. Merki, H. Vrubel, L. Rovelli, S. Fierro, X. Hu, *Chem. Sci.* **2012**, *3*, 2515.
[47] J. Bonde, P. G. Moses, T. F. Jaramillo, J. K. Norskov, I. Chorkendorff, *Faraday Discuss.* **2009**, *140*, 219.
[48] Q. Gong, L. Cheng, C. Liu, M. Zhang, Q. Feng, H. Ye, M. Zeng, L. Xie, Z. Liu, Y. Li, *ACS Catal.* **2015**, *5*, 2213.
[49] L. Yang, Q. Fu, W. Wang, J. Huang, J. Huang, J. Zhang, B. Xiang, *Nanoscale* **2015**, *7*, 10490.
[50] K. Xu, F. Wang, Z. Wang, X. Zhan, Q. Wang, Z. Cheng, M. Safdar, J. He, *ACS Nano* **2014**, *8*, 8468
[51] K. Wang, C. Zhou, D. Xi, Z. Shi, C. He, H. Xia, G. Liu, G. Qiao, *Nano Energy* **2015**, *18*, 1.
[52] F. Wang, J. Li, F. Wang, T. A. Shifa, Z. Cheng, Z. Wang, K. Xu, X. Zhan, Q. Wang, Y. Huang, C. Jiang, J. He, *Adv. Funct. Mater.* **2015**, *25*, 6077.

[53] K. Liu, F. Wang, K. Xu, T. A. Shifa, Z. Cheng, X. Zhan, J. He, *Nanoscale* **2016**, *8*, 4699.

[54] X. Dai, K. Du, Z. Li, M. Liu, Y. Ma, H. Sun, X. Zhang, Y. Yang, *ACS Appl. Mater. Interfaces* **2015**, *7*, 27242.

[55] T. Kubota, N. Miyamoto, M. Yoshioka, Y. Okamoto, *Appl. Catal. A: General* **2014**, *480*, 10.

[56] M. J. Vissenberg, Y. van der Meer, E. J. M. Hensen, V. H. J. de Beer, A. M. van der Kraan, R. A. van Santen, J. A. R. van Veen, *J. Catal.* **2001**, *198*, 151.

[57] T. A. Shifa, F. Wang, Z. Cheng, X. Zhan, Z. Wang, K. Liu, M. Safdar, L. Sun, J. He, *Nanoscale* **2015**, *7*, 14760.

[58] X. Zhan, Z. Wang, F. Wang, Z. Cheng, K. Xu, Q. Wang, M. Safdar, J. He, *Appl. Phys. Lett.* **2014**, *105*, 153903.

[59] M. Zhang, J. Wu, Y. Zhu, D. O. Dumcenco, J. Hong, N. Mao, S. Deng, Y. Chen, Y. Yang, C. Jin, S. H. Chaki, Y.-S. Huang, J. Zhang, L. Xie, *ACS Nano* **2014**, *8*, 7130.

[60] C. Ouyang, X. Wang, S. Wang, *Chem. Commun.* **2015**, *51*, 14160.

[61] Z. Wang, P. Liu, Y. Ito, S. Ning, Y. Tan, T. Fujita, A. Hirata, M. Chen, *Sci. Rep.* **2016**, *6*, 21536.

[62] A. D. Gandubert, C. Legens, D. Guillaume, E. Payen, *Surf. Interface Anal.* **2006**, *38*, 206.

[63] A. D. Gandubert, E. Krebs, C. Legens, D. Costa, D. Guillaume, P. Raybaud, *Catal. Today* **2008**, *130*, 149.

[64] A. D. Gandubert, C. Legens, D. Guillaume, S. Rebours, E. Payen, *Oil Gas Sci.Technol.—Revue de l'IFP* **2007**, *62*, 79.

[65] T. C. Kaspar, T. Droubay, S. M. Heald, M. H. Engelhard, P. Nachimuthu, S. A. Chambers, *Phys. Rev. B* **2008**, 77.

[66] C. C. Wang, M. Liu, B. Y. Man, C. S. Chen, S. Z. Jiang, S. Y. Yang, X. G. Gao, S. C. Xu, B. Hu, Z. C. Sun, J. J. Guo, J. Hou, *AIP Adv.* **2012**, *2*, 012182.

[67] L. A. Kibler, *ChemPhysChem* **2006**, *7*, 985.

[68] L. Cheng, W. Huang, Q. Gong, C. Liu, Z. Liu, Y. Li, H. Dai, *Angew. Chem. Int. Ed.* **2014**, *53*, 7860.

[69] H. Du, S. Gu, R. Liu, C. M. Li, *J. Power Sources* **2015**, *278*, 540.

[70] J. M. McEnaney, J. C. Crompton, J. F. Callejas, E. J. Popczun, C. G. Read, N. S. Lewis, R. E. Schaak, *Chem. Commun.* **2014**, *50*, 11026.

[71] Z. Xing, Q. Liu, A. M. Asiri, X. Sun, *ACS Catal.* **2015**, *5*, 145.

[72] S. Yu, J. Kim, K. R. Yoon, J. W. Jung, J. Oh, I. D. Kim, *ACS Appl. Mater. Interfaces* **2015**, *7*, 28116.

[73] J. Yang, D. Voiry, S. J. Ahn, D. Kang, A. Y. Kim, M. Chhowalla, H. S. Shin, *Angew. Chem. Int. Ed* **2013**, *52*, 13751.

[74] G.-Q. Han, Y.-R. Liu, W.-H. Hu, B. Dong, X. Li, Y.-M. Chai, Y.-Q. Liu, C.-G. Liu, *Mater. Chem. Phys.* **2015**, *167*, 271.

[75] J. Lin, Z. Peng, G. Wang, D. Zakhidov, E. Larios, M. J. Yacaman, J. M. Tour, *Adv. Energy Mater.* **2014**, *4*, 1301875.

[76] Z. Pu, Q. Liu, A. M. Asiri, X. Sun, *ACS Appl. Mater. Interfaces* **2014**, *6*, 21874.

[77] B. Seo, H. Y. Jeong, S. Y. Hong, A. Zak, S. H. Joo, *Chem. Commun.* **2015**, *51*, 8334.

[78] Y. Yan, B. Xia, N. Li, Z. Xu, A. Fisher, X. Wang, *J. Mater. Chem. A* **2015**, *3*, 131.